Measurement of $R = \sigma_L/\sigma_T$ in Deep-Inelastic Scattering on Nuclei

A. Airapetian,[31] N. Akopov,[31] Z. Akopov,[31] M. Amarian,[26,31] V.V. Ammosov,[24] E.C. Aschenauer,[6] R. Avakian,[31] A. Avetissian,[31] E. Avetissian,[31] P. Bailey,[15] V. Baturin,[23] C. Baumgarten,[21] M. Beckmann,[5] S. Belostotski,[23] S. Bernreuther,[29] N. Bianchi,[10] H.P. Blok,[22,30] H. Böttcher,[6] A. Borissov,[19] O. Bouhali,[22] M. Bouwhuis,[15] J. Brack,[4] S. Brauksiepe,[11] A. Brüll,[18] I. Brunn,[8] G.P. Capitani,[10] H.C. Chiang,[15] G. Ciullo,[9] G.R. Court,[16] P.F. Dalpiaz,[9] R. De Leo,[3] L. De Nardo,[1] E. De Sanctis,[10] E. Devitsin,[20] P.K.A. de Witt Huberts,[22] P. Di Nezza,[10] M. Düren,[13] M. Ehrenfried,[6] A. Elalaoui-Moulay,[2] G. Elbakian,[31] F. Ellinghaus,[6] U. Elschenbroich,[11] J. Ely,[4] R. Fabbri,[9] A. Fantoni,[10] A. Fechtchenko,[7] L. Felawka,[28] H. Fischer,[11] B. Fox,[4] J. Franz,[11] S. Frullani,[26] Y. Gärber,[8] G. Gapienko,[24] V. Gapienko,[24] F. Garibaldi,[26] E. Garutti,[22] G. Gavrilov,[23] V. Gharibyan,[31] G. Graw,[21] O. Grebeniouk,[23] P.W. Green,[1,28] L.G. Greeniaus,[1,28] A. Gute,[8] W. Haeberli,[17] K. Hafidi,[2] M. Hartig,[28] D. Hasch,[10] D. Heesbeen,[22] F.H. Heinsius,[11] M. Henoch,[8] R. Hertenberger,[21] W.H.A. Hesselink,[22,30] Y. Holler,[5] B. Hommez,[12] G. Iarygin,[7] A. Izotov,[23] H.E. Jackson,[2] A. Jgoun,[23] R. Kaiser,[14] E. Kinney,[4] A. Kisselev,[23] P. Kitching,[1] K. Königsmann,[11] H. Kolster,[18] M. Kopytin,[23] V. Korotkov,[6] E. Kotik,[1] V. Kozlov,[20] B. Krauss,[8] V.G. Krivokhijine,[7] L. Lagamba,[3] L. Lapikás,[22] A. Laziev,[22,30] P. Lenisa,[9] P. Liebing,[6] T. Lindemann,[5] W. Lorenzon,[19] N.C.R. Makins,[15] H. Marukyan,[31] F. Masoli,[9] F. Menden,[11] V. Mexner,[22] N. Meyners,[5] O. Mikloukho,[23] C.A. Miller,[1,28] V. Muccifora,[10] A. Nagaitsev,[7] E. Nappi,[3] Y. Naryshkin,[23] A. Nass,[8] K. Negodaeva,[6] W.-D. Nowak,[6] K. Oganessyan,[5,10] H. Ohsuga,[29] G. Orlandi,[26] S. Podiatchev,[8] S. Potashov,[20] D.H. Potterveld,[2] M. Raithel,[8] D. Reggiani,[9] P.E. Reimer,[2] A. Reischl,[22] A.R. Reolon,[10] K. Rith,[8] G. Rosner,[14] A. Rostomyan,[31] D. Ryckbosch,[12] Y. Sakemi,[29] I. Sanjiev,[2,23] F. Sato,[29] I. Savin,[7] C. Scarlett,[19] A. Schäfer,[25] C. Schill,[11] G. Schnell,[6] K.P. Schüler,[5] A. Schwind,[6] J. Seibert,[11] B. Seitz,[1] R. Shanidze,[8] T.-A. Shibata,[29] V. Shutov,[7] M.C. Simani,[22,30] K. Sinram,[5] M. Stancari,[9] M. Statera,[9] E. Steffens,[8] J.J.M. Steijger,[22] J. Stewart,[6] U. Stösslein,[4] K. Suetsugu,[29] H. Tanaka,[29] S. Taroian,[31] A. Terkulov,[20] S. Tessarin,[9] E. Thomas,[10] A. Tkabladze,[6] M. Tytgat,[12] G.M. Urciuoli,[26] G. van der Steenhoven,[22] R. van de Vyver,[12] M.C. Vetterli,[27,28] V. Vikhrov,[23] M.G. Vincter,[1] J. Visser,[22] J. Volmer,[6] C. Weiskopf,[8] J. Wendland,[27,28] J. Wilbert,[8] T. Wise,[17] S. Yen,[28] S. Yoneyama,[29] B. Zihlmann,[22,30] and H. Zohrabian[31]

(The HERMES Collaboration)

[1]*Department of Physics, University of Alberta, Edmonton, Alberta T6G 2J1, Canada*
[2]*Physics Division, Argonne National Laboratory, Argonne, Illinois 60439-4843, USA*
[3]*Istituto Nazionale di Fisica Nucleare, Sezione di Bari, 70124 Bari, Italy*
[4]*Nuclear Physics Laboratory, University of Colorado, Boulder, Colorado 80309-0446, USA*
[5]*DESY, Deutsches Elektronen-Synchrotron, 22603 Hamburg, Germany*
[6]*DESY Zeuthen, 15738 Zeuthen, Germany*
[7]*Joint Institute for Nuclear Research, 141980 Dubna, Russia*
[8]*Physikalisches Institut, Universität Erlangen-Nürnberg, 91058 Erlangen, Germany*
[9]*Istituto Nazionale di Fisica Nucleare, Sezione di Ferrara and Dipartimento di Fisica, Università di Ferrara, 44100 Ferrara, Italy*
[10]*Istituto Nazionale di Fisica Nucleare, Laboratori Nazionali di Frascati, 00044 Frascati, Italy*
[11]*Fakultät für Physik, Universität Freiburg, 79104 Freiburg, Germany*
[12]*Department of Subatomic and Radiation Physics, University of Gent, 9000 Gent, Belgium*
[13]*Physikalisches Institut, Universität Gießen, 35392 Gießen, Germany*
[14]*Department of Physics and Astronomy, University of Glasgow, Glasgow G128 QQ, United Kingdom*
[15]*Department of Physics, University of Illinois, Urbana, Illinois 61801, USA*
[16]*Physics Department, University of Liverpool, Liverpool L69 7ZE, United Kingdom*
[17]*Department of Physics, University of Wisconsin-Madison, Madison, Wisconsin 53706, USA*
[18]*Laboratory for Nuclear Science, Massachusetts Institute of Technology, Cambridge, Massachusetts 02139, USA*
[19]*Randall Laboratory of Physics, University of Michigan, Ann Arbor, Michigan 48109-1120, USA*
[20]*Lebedev Physical Institute, 117924 Moscow, Russia*
[21]*Sektion Physik, Universität München, 85748 Garching, Germany*
[22]*Nationaal Instituut voor Kernfysica en Hoge-Energiefysica (NIKHEF), 1009 DB Amsterdam, The Netherlands*
[23]*Petersburg Nuclear Physics Institute, St. Petersburg, Gatchina, 188350 Russia*
[24]*Institute for High Energy Physics, Protvino, Moscow oblast, 142284 Russia*
[25]*Institut für Theoretische Physik, Universität Regensburg, 93040 Regensburg, Germany*
[26]*Istituto Nazionale di Fisica Nucleare, Sezione Roma 1, Gruppo Sanità and Physics Laboratory, Istituto Superiore di Sanità, 00161 Roma, Italy*
[27]*Department of Physics, Simon Fraser University, Burnaby, British Columbia V5A 1S6, Canada*
[28]*TRIUMF, Vancouver, British Columbia V6T 2A3, Canada*

[29]Department of Physics, Tokyo Institute of Technology, Tokyo 152, Japan
[30]Department of Physics and Astronomy, Vrije Universiteit, 1081 HV Amsterdam, The Netherlands
[31]Yerevan Physics Institute, 375036 Yerevan, Armenia
(Dated: February 6, 2008)

Cross section ratios for deep-inelastic scattering from ^{3}He, ^{14}N and ^{84}Kr with respect to ^{2}H have been measured by the HERMES collaboration at DESY using a 27.5 GeV positron beam. The data cover a range in the Bjorken scaling variable x between 0.010 and 0.65, the negative squared four-momentum transfer Q^2 varies from 0.5 to 15 GeV^2, while at small values of x and Q^2, the virtual photon polarisation parameter ϵ extends to lower values than previous measurements. From the dependence of the data on ϵ, values for R_A/R_D with R the ratio σ_L/σ_T of longitudinal to transverse DIS cross sections have been derived and found to be consistent with unity.

In 1993 the EMC collaboration published a significant difference between the deep-inelastic scattering (DIS) cross sections per nucleon on iron and deuterium [1], indicating that the quark momentum distributions in bound nucleons differ from those in free nucleons. This phenomenon is known as the *EMC effect* at large values of the Bjorken scaling variable $x (x > 0.1)$, and as *shadowing* at lower values of x [2].

With $F_2(x)$ found to be A-dependent, it is relevant to investigate whether this dependence is the same for its longitudinal and transverse components, $F_L(x)$ and $F_1(x)$. The latter two structure functions are related to $F_2(x)$ via $F_L(x) = (1+Q^2/\nu^2)F_2(x) - 2xF_1(x)$ with $-Q^2$ the square of the four-momentum transfer, ν the energy transfer, $x = Q^2/2M\nu$ and M the nucleon mass. A possible difference between the A-dependences of $F_L(x)$ and $F_1(x)$ can be investigated by measuring the ratio of longitudinal to transverse deep-inelastic scattering cross sections $R = \sigma_L/\sigma_T = F_L(x)/2xF_1(x)$ for various nuclear targets. While several such studies have been reported [3, 4, 5], none of these has provided values of R in the kinematic regime $x < 0.06$ with $Q^2 < 1\,\mathrm{GeV}^2$. This region is the focus of the present paper.

In deep-inelastic charged lepton scattering from an unpolarised target, the double-differential cross section per nucleon can be written in the one-photon exchange approximation as

$$\begin{aligned}\frac{d^2\sigma}{dxdQ^2} &= \frac{4\pi\alpha^2}{Q^4}\frac{F_2(x,Q^2)}{x} \times \\ &\quad \left[1 - y - \frac{Q^2}{4E^2} + \frac{y^2}{2}\left(\frac{1+Q^2/\nu^2}{1+R(x,Q^2)}\right)\right] \\ &= \frac{\sigma_{\mathrm{Mott}}}{E'E}\frac{\pi F_2(x,Q^2)}{x\epsilon}\frac{1+\epsilon R(x,Q^2)}{1+R(x,Q^2)}, \qquad (1)\end{aligned}$$

where $y = \nu/E$, σ_{Mott} represents the cross section for lepton scattering from a point charge, and E and E' are the initial and final lepton energies in the target rest frame, respectively. The virtual photon polarisation parameter is given by

$$\epsilon = \frac{4(1-y) - Q^2/E^2}{4(1-y) + 2y^2 + Q^2/E^2}. \qquad (2)$$

The ratio of DIS cross sections on nucleus A and deuterium D (=^{2}H) is then given by:

$$\frac{\sigma_A}{\sigma_D} = \frac{F_2^A}{F_2^D}\frac{(1+\epsilon R_A)(1+R_D)}{(1+R_A)(1+\epsilon R_D)}, \qquad (3)$$

where R_A and R_D represent the ratio σ_L/σ_T for nucleus A and deuterium. To facilitate easier interpretation and in accordance to the literature, here and throughout this paper all cross sections are defined as cross sections per nucleon and are converted to cross sections for isoscalar nuclei, i.e. the measured cross sections are divided by the atomic number A and corrected for any difference in the number of protons and neutrons:

$$\frac{\sigma_A}{\sigma_D} \equiv \frac{\sigma_A^{nucleus}}{Z\sigma_p + (A-Z)\sigma_n}, \qquad (4)$$

where $\sigma_A^{nucleus}$ is the DIS cross section per nucleus for nucleus A and σ_p and σ_n are the DIS cross sections on the proton and the neutron. In practice, $\sigma_A^{nucleus}/\sigma_D$ is converted to σ_A/σ_D using the known cross section ratio σ^D/σ^p [6].

For $\epsilon \to 1$ the cross section ratio equals the ratio of structure functions F_2^A/F_2^D. For smaller values of ϵ the cross section ratio is equal to F_2^A/F_2^D only if $R_A = R_D$. A difference between R_A and R_D will thus introduce an ϵ-dependence of σ_A/σ_D. Hence, measurements of σ_A/σ_D as a function of ϵ can be used to extract experimental information on R_A/R_D, if R_D is known.

In this paper we present data from the HERMES experiment on the cross section ratio for deep-inelastic positron scattering off helium-3, nitrogen and krypton with respect to deuterium. The helium-3 and nitrogen data were published in a previous letter [7]. Recently, those data were found to be subject to an A-dependent tracking inefficiency of the HERMES spectrometer [8], which was not recognised in the previous analysis. The resulting correction of the cross section ratios is significant at low values of x and Q^2 and substantially changes the interpretation of those data. The data presented here were corrected for this effect and supersede those published in Ref. [7].

The data were collected by the HERMES experiment at DESY using ^{1}H, ^{2}H, ^{3}He, ^{14}N and ^{84}Kr molecular gas targets internal to the 27.5 GeV positron storage ring

of HERA. The target gases were injected into a 40 cm long, tubular open-ended storage cell inside the positron ring. The luminosity was measured by detecting Bhabha-scattered target electrons in coincidence with the scattered positrons, in a pair of $NaBi(WO_4)_2$ electromagnetic calorimeters.

The HERMES spectrometer [9] is a forward angle instrument which is symmetric about a central horizontal shielding plate in the magnet. Both the scattered positrons and the hadrons produced can be detected and identified within an angular acceptance of ± 170 mrad horizontally, and 40 – 140 mrad vertically. The trigger was formed from a coincidence between signals of three scintillator hodoscope planes and a lead-glass calorimeter where a minimum energy deposit of 3.5 GeV was required. Positron identification was accomplished using the calorimeter, the second hodoscope, which functioned as a preshower counter, a transition-radiation detector and a Čerenkov counter. This system provided positron identification with an average efficiency of 99 % and a hadron contamination of less than 1 %.

Deep-inelastic scattering events were extracted from the data by imposing constraints on Q^2 ($Q^2 > 0.3$ GeV^2), W (the invariant mass of the photon-nucleon system, required to be greater than 2 GeV), and y ($y < 0.85$). At very low x and high y, the nuclear cross sections are dominated by radiative processes associated with elastic scattering. To limit these contributions, a minimum x value of $x = 0.01$ was required.

As the ratio σ_A/σ_D involves nuclei with different numbers of protons, radiative corrections do not cancel in the ratio. In particular, the yield of radiative processes associated with elastic scattering scales with Z^2 and thus differs for the two target nuclei. At small values of apparent x and Q^2 (inferred from the kinematics of the scattered positron), corresponding to large values of y, the contribution from radiative elastic scattering becomes large. In this kinematic region, the associated energetic photons radiated at small angles can produce electromagnetic showers that cause large tracking inefficiencies [8]. Corrections for these process-specific inefficiencies must be applied, since they increase in severity as the Z of nuclear targets increases.

These track reconstruction losses in the HERMES detector have been simulated in detail using the GEANT-based Monte Carlo description of the experiment. The probability of photon emission is modelled following the description of Mo and Tsai [10], and has been carefully compared to other calculations of radiative processes. All materials close to the beam pipe have been implemented in detail and the effect of the minimum energy of the secondary particles tracked through the detector was investigated. The resulting reconstruction losses at low x and Q^2 strongly depend on the target material and show a strong variation with y, and consequently with x and Q^2. The ratios of the reconstruction efficiencies η for target nucleus A compared to deuterium are shown in Fig. 1 as a function of x, for the various target materials used in the HERMES experiment. For completeness, this figure includes points at smaller values of x than are employed in the present analysis.

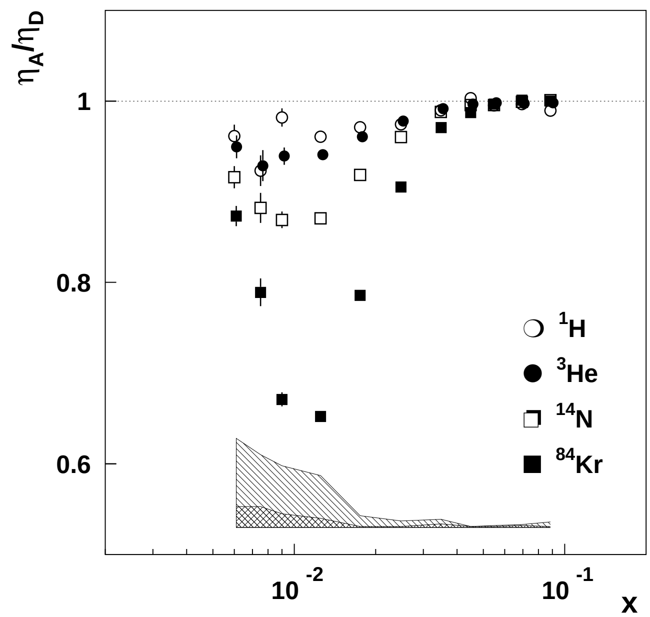

FIG. 1: Ratio of track reconstruction efficiencies in ^{1}H, ^{3}He, ^{14}N and ^{84}Kr with respect to ^{2}H as function of x. The hatched areas represent the systematic uncertainties for the N/D (cross hatched) and Kr/D (slanted hatched) efficiency ratios. The systematic uncertainties for the H/D and He/D ratios are smaller than that of the N/D ratio and are not shown.

The systematic uncertainty of this correction was estimated using the fact that the HERMES spectrometer consists of two independent detectors above and below the positron beam. For about 50 % of the events with a hard radiated photon the resulting electromagnetic shower is contained in one detector while the scattered electron is found in the other detector. While these events are rejected by the standard HERMES reconstruction algorithm because of their high total multiplicity, they can be reconstructed when one considers the two detectors independently. The number of events gained in this way strongly depends on the details of the electromagnetic shower – especially on the energy of the radiated photon and the exact position where the photon hits any material – and thus provides a good measure of the quality of the MC simulation. Reasonable agreement between the data and the simulation is found for all target materials. Fig. 2 shows as a function of apparent x the fractional change in the yield ratios when treating the upper and lower spectrometer halves independently, both for the data and the MC simulation. Here the yields from

the two detector halves have been averaged. A difference between the yields in the upper and the lower detector observed in the data is attributed to a relative misalignment between the two detectors. As is typical practice for combining results which are statistically incompatible [11], the statistical uncertainty of the weighted mean is scaled by the square root of χ^2. The difference between the yields in the two detectors is significant only in the krypton data at low x ($x < 0.03$) where the reconstruction efficiency quickly changes with x and the difference can be up to 10 %. The difference between the data and the MC simulation is treated as a systematic uncertainty.

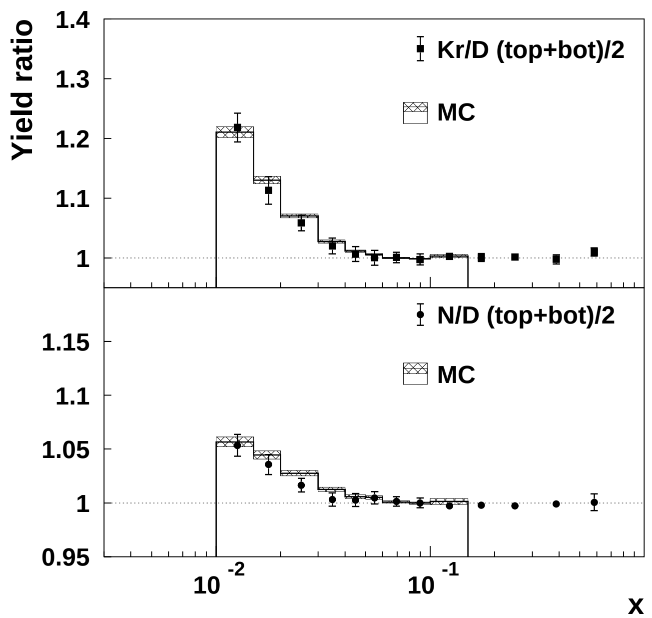

FIG. 2: Comparison between data (points) and MC simulation (histogram) for the fractional change in the cross section ratios when treating the upper and lower HERMES detector halves independently.

The track reconstruction inefficiency mainly affects radiative elastic and to some extent quasielastic events. These and all other radiative processes have been computed using the method outlined in Ref. [12]. For the evaluation of the coherent radiative tails, the nuclear elastic form factors must be known. Parameterisations of the form factors of ^{2}H, ^{3}He, ^{14}N and ^{84}Kr were taken from the literature [13, 14, 15, 16]. For the quasi-elastic tails, the nucleon form factor parameterisation of Gari and Krümpelmann [17] was used. The reduction of the bound nucleon cross section with respect to the free nucleon one (quasi-elastic suppression) was evaluated using the results of a calculation by Bernabeu [18] for deuterium and the non-relativistic Fermi gas model for ^{3}He, ^{14}N and ^{84}Kr [19]. The evaluation of the inelastic QED processes requires the knowledge of both F_2 and R over a wide range of x and Q^2. The structure function $F_2^D(x, Q^2)$ was described by a Regge motivated parameterisation of the proton structure function $F_2^p(x, Q^2)$ [20] multiplied by the NMC measurement of F_2^D/F_2^p [6]; for R_D the Whitlow parameterisation [21] was used. The nuclear structure functions $F_2^A(x, Q^2)$ were taken from phenomenological fits to the SLAC and NMC data, and $R_A(x, Q^2)$ was assumed to be equal to $R_D(x, Q^2)$. The effects of all radiative processes were subtracted from the measured yields and the statistical errors propagated accordingly. This method avoids the possible large model dependence that can result from multiplicatively applying radiative corrections [22]. Because of the reconstruction inefficiency explained above, only those radiative events actually seen by the HERMES spectrometer were subtracted.

For high-Z targets such as krypton, the probability for the exchange of more than one photon becomes non-negligible. The corresponding amplitudes lead to a destructive interference with the leading amplitudes. For the dominant contribution to the radiative corrections — the coherent radiative tail — this effect has been estimated using the distorted wave function method [23], resulting into a 5-10 % reduction of the radiative elastic tail. Other contributions proportional to $Z \cdot \alpha_{EM}$ might be non-negligible but could not be estimated.

The systematic uncertainty in the radiative corrections was estimated by using upper and lower limits of the parameterisations, or alternative parameterisations [21, 24, 25, 26] for all the above input parameters. The resulting systematic uncertainty in the cross section ratio of Kr/D is about 6 % at low x, quickly falling to values smaller than 1 % for $x > 0.06$. (As mentioned before this uncertainty does not include the effects of multiphoton exchange (Coulomb distortion) beyond the estimated contribution to the coherent elastic tail; these contributions might be non-negligible but could not be estimated.) Because of the smaller radiative contributions, the uncertainties due to the radiative corrections in the cross section ratios of nitrogen and helium with respect to deuterium are about 3 % at low x.

The effects originating from the finite resolution of the spectrometer and from the hadron contamination in the positron sample have been determined and found to be negligible. The overall normalisation uncertainty has been estimated from the luminosity measurements to be 1.4 % for the He(N)/D data and 1 % for the Kr/D data.

The results of the present analysis [27] are shown in Fig. 3 as a function of x. Also shown are the results of the NMC [28, 29, 30] and SLAC [31] measurements of σ_{He}/σ_D, σ_C/σ_D and σ_{Sn}/σ_D where the NMC values for σ_{Sn}/σ_D have been obtained from the measurements of σ_{Sn}/σ_C and σ_C/σ_D. On average, the present data on σ_{He}/σ_D and σ_N/σ_D are about 0.9 % below the cross section ratio reported by NMC. A similar difference is observed in comparison to the SLAC data which cover a smaller x but the same Q^2 range than the HERMES data. As the normalisation uncertainty of the present data is

considerably larger than that of the NMC data (0.4 %), the σ_{He}/σ_D and σ_N/σ_D results have been renormalised by 0.9 %. No such renormalisation has been applied to the Kr/D cross section ratios. For x values below $x = 0.1$, the present data on N/D and Kr/D are slightly below the NMC data but consistent within the present statistical and systematic uncertainties.

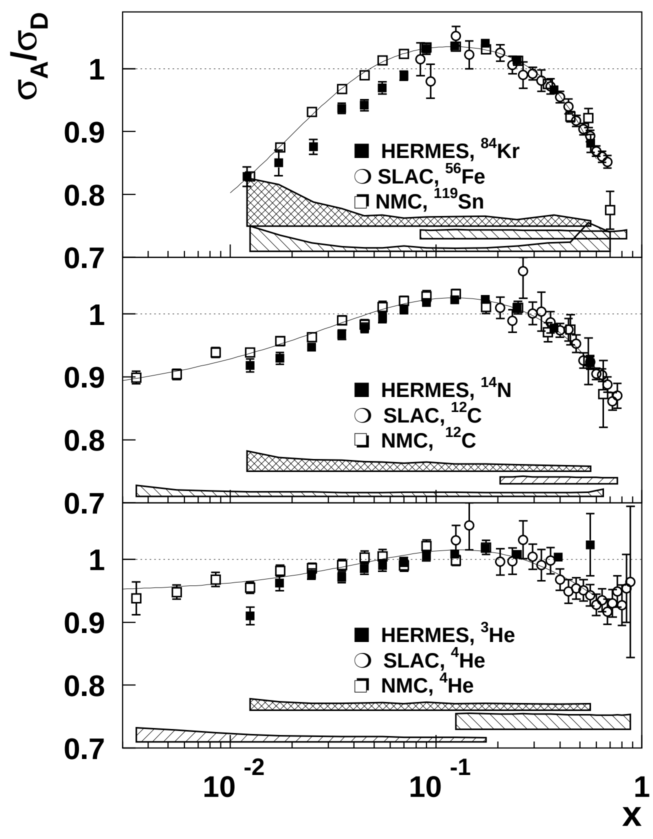

FIG. 3: Ratio of isoscalar Born cross sections of inclusive deep-inelastic lepton scattering from nucleus A and D versus x. The error bars represent the statistical uncertainties, the systematic uncertainties are given by the error bands. The HERMES ^{3}He/D and ^{14}N/D data have been renormalised by 0.9 %.

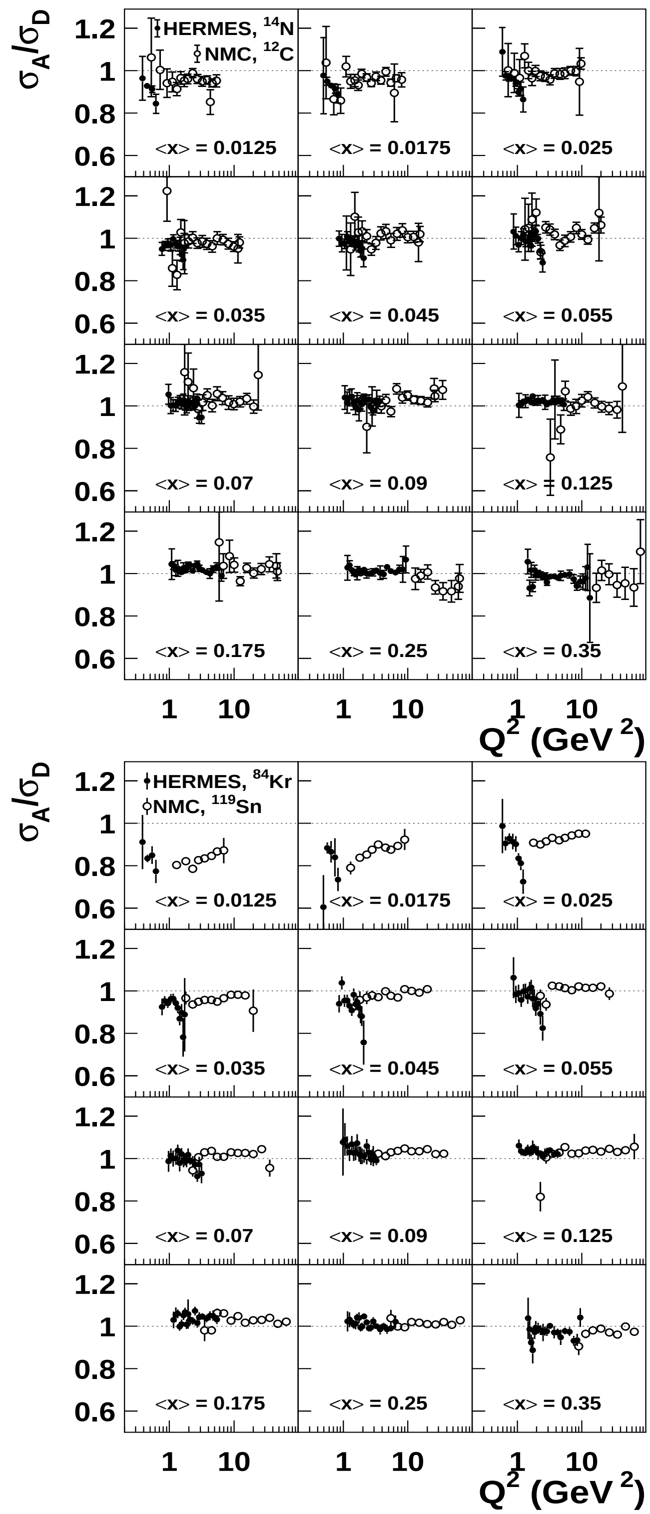

FIG. 4: Ratio of isoscalar Born cross sections of inclusive deep-inelastic lepton scattering from nucleus A and D as function of Q^2 for fixed values of x. The error bars represent the statistical uncertainties. The HERMES ^{14}N/D data have been renormalised by 0.9 %.

The small discrepancy between the HERMES Kr/D and the NMC Sn/D data at $0.02 < x < 0.08$ is likely due to the positive Q^2 dependence observed in the NMC Sn/D data. This is better illustrated in Fig. 4 where the σ_N/σ_D and σ_{Kr}/σ_D data are displayed as function of Q^2 for fixed values of x together with the NMC data on σ_C/σ_D and σ_{Sn}/σ_D respectively. For x values below $x = 0.08$, the NMC data on σ_{Sn}/σ_D show a significant positive Q^2 dependence resulting into a difference between the cross section ratio at the average Q^2 of the NMC data (as displayed in Fig. 3) and at the average Q^2 of the HERMES data. While no significant Q^2 dependence is observed in the cross section ratio of ^{14}N/D, the large uncertainties in the HERMES Kr/D data do not allow to distinguish between a flat Q^2 dependence and an extrapolation of the small positive Q^2 dependence observed in the NMC measurement of σ_{Sn}/σ_D.

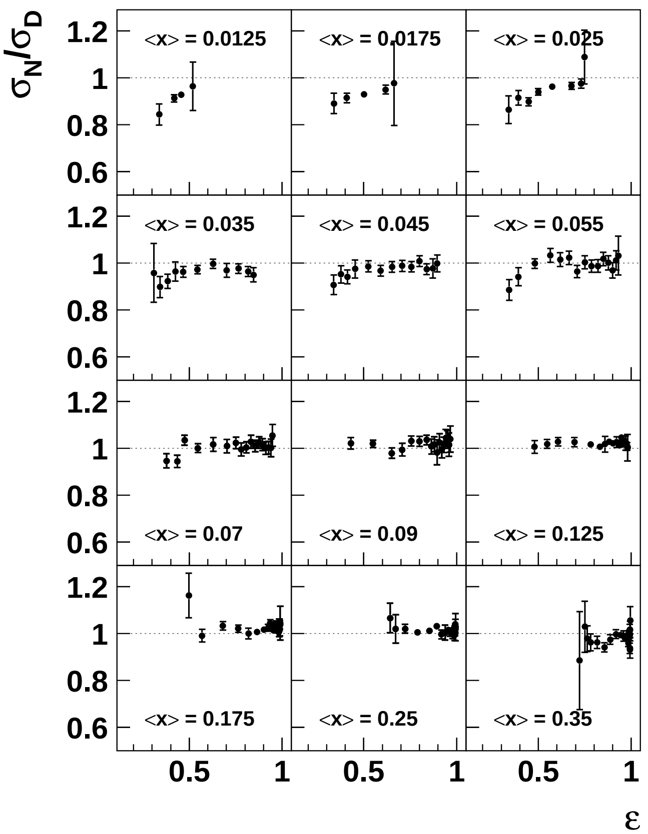

FIG. 5: Ratio of isoscalar Born cross sections of inclusive deep-inelastic lepton scattering from nitrogen and deuterium (renormalised by 0.9 %) as function of ϵ for fixed values of x. The error bars represent the statistical uncertainties.

To investigate a possible A-dependence of $R(x, Q^2)$, the cross section ratios have been fitted as a function of ϵ for fixed values of x (Eq. 3). In these fits a parameterisation of R_D [21] has been used, while the ratios R_A/R_D and F_2^A/F_2^D have been treated as free parameters. A single value of R_A/R_D and F_2^A/F_2^D has been extracted from each x-bin. In this procedure it is assumed that both R_A/R_D and F_2^A/F_2^D are constant over the limited Q^2 range covered by the data in each x-bin. The ϵ-dependence of the ^{14}N/D cross section ratio is shown in Fig. 5. No sigificant ϵ-dependence is observed. Similar conclusions hold for the other target nuclei.

The values of F_2^A/F_2^D derived from the fit of the HERMES data are found to be consistent with previous measurements of NMC and SLAC. The resulting values of R_A/R_D are shown in Fig. 6. Also shown are the results of previous studies of the A-dependence of R. Existing data are usually represented in terms of $\Delta R = R_A - R_D$. The published values of ΔR [3, 4, 5] have been converted to R_A/R_D using a parameterisation for R_D [21], and added to Fig. 6. All data are found to be consistent with unity.

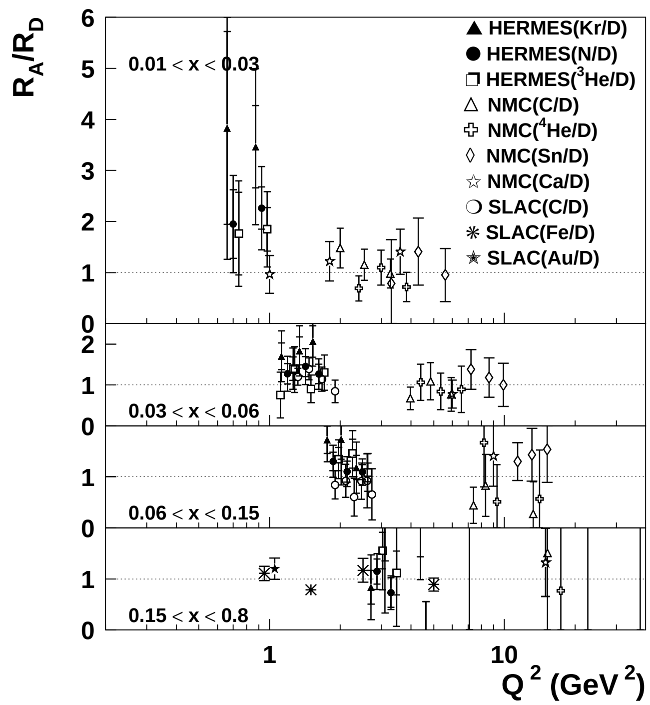

FIG. 6: The isoscalar-corrected ratio R_A/R_D for several nuclei (A) with respect to deuterium as a function of Q^2 for four different x bins. The open triangles (^{12}C) and crosses (^{4}He) have been derived from the NMC data using Eq. 3. The other SLAC [4] and NMC data [5] displayed have been derived from published values of $\Delta R = R_A - R_D$ and a parameterisation [21] for R_D. The inner error bars represent the statistical uncertainty and include the correlated error in F_2^A/F_2^D. The outer error bars represent the quadratic sum of the statistical and systematic uncertainties. In the upper panel the HERMES results at the lowest Q^2 value have been suppressed because of its large error bar.

At low x, the HERMES cross section ratios on ^{3}He and ^{14}N and the NMC measurements on ^{4}He and ^{12}C have some common Q^2 range. While the NMC measurements at these x and Q^2 values have ϵ values close to unity, the HERMES data cover a typical ϵ range of $0.4 < \epsilon < 0.7$.

Combining the two measurements thus increases the precision on R_A/R_D. Because of the different experimental conditions of the NMC measurements on the heavy targets no such overlap in x and Q^2 exists for the HERMES krypton data and the NMC data on iron or tin. Therefore the determination of R_A/R_D on heavy nuclei is not improved by combining the HERMES and NMC data. The results of the fits to the HERMES and NMC data on helium and nitrogen (carbon) are displayed in Fig. 7 as a function of Q^2 together with all other measurements of R_A/R_D on light and medium heavy nuclei. For Q^2 values between 0.5 and 20 GeV^2 and nuclei from He to Ca, R_A is found to be consistent with the R parametrisation of Whitlow et al [21]. As throughout this paper, this R parametrisation has been choosen in this comparison because it is dominated by data on the proton and the deuteron. In contrast, the more recent parametrisation by Abe et al. [3] is significantly influenced by nuclear data. The influence of the choice in the R parametrisation is however very small. Averaging over all measurements of R_A/R_D for light and medium heavy nuclei gives an average value for R_A/R_D of 0.99 ± 0.03, a result which is unchanged if the data on the heavier nuclei are included in the average.

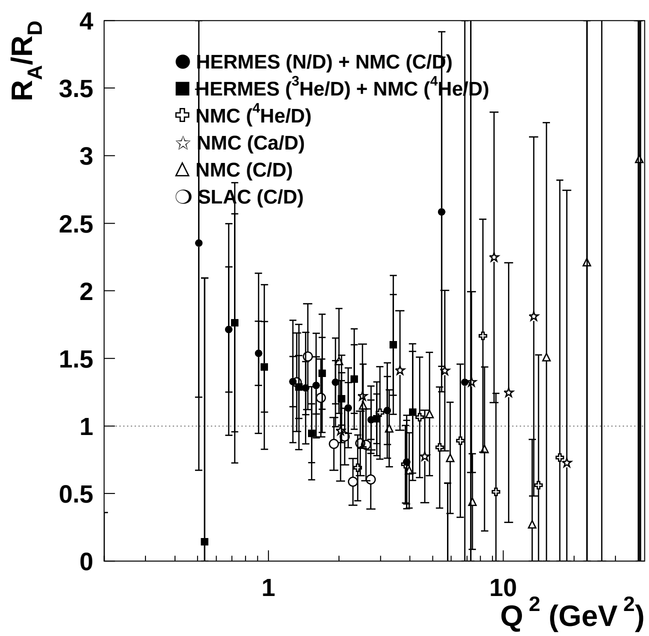

FIG. 7: The isoscalar-corrected ratio R_A/R_D for several nuclei (A) with respect to deuterium as a function of Q^2. The HERMES and NMC data have been combined in the determination of R_A/R_D. The other data are the same as in Fig. 6.

In summary, deep-inelastic positron scattering data on ^{2}H, ^{3}He, ^{14}N and ^{84}Kr are presented. The results extracted for the ratios of the DIS cross sections on nuclei to those on the corresponding sets of free nucleons is in good agreement with the results from previous measurements, after the data were corrected for a previously unrecognised A-dependent tracking inefficiency. No significant Q^2 dependence is observed over the wide range in Q^2 covered by the combined data set of HERMES and NMC. Values for the ratio of R_A/R_D with R the ratio σ_L/σ_T of longitudinal to transverse DIS cross sections have been derived from the dependence of the data on the virtual photon polarisation parameter ϵ and found to be consistent with unity. The data presented in this paper extend the kinematic range in which R_A is found to be equal to R_D down to $x = 0.01$ and $Q^2 = 0.5$ GeV^2.

We gratefully acknowledge the DESY management for its support and the DESY staff and the staffs of the collaborating institutions. This work was supported by the FWO-Flanders, Belgium; the Natural Sciences and Engineering Research Council of Canada; the INTAS contribution from the European Commission; the European Commission IHP program under contract HPRN-CT-2000-00130; the German Bundesministerium für Bildung und Forschung (BMBF); the Deutscher Akademischer Austauschdienst (DAAD); the Italian Istituto Nazionale di Fisica Nucleare (INFN); Monbusho International Scientific Research Program, JSPS, and Toray Science Foundation of Japan; the Dutch Foundation for Fundamenteel Onderzoek der Materie (FOM); the U.K. Particle Physics and Astronomy Research Council; and the U.S. Department of Energy and National Science Foundation.

[1] J.J. Aubert et al. (EMC), Phys. Lett. B **123** (1983) 275.
[2] M. Arneodo, Phys. Rep. **240** (1994) 301.
[3] K. Abe et al. (SLAC), Phys. Lett. B **452** (1999) 194.
[4] S. Dasu et al. (SLAC), Phys. Rev. D **49** (1994) 5641.
[5] P. Amaudruz et al. (NMC), Phys. Lett. B **294** (1992) 120; and M. Arneodo et al. (NMC), Phys. Lett. B **481** (1996) 23.
[6] M. Arneodo et al. (NMC), Nucl. Phys. B **487** (1997) 3.
[7] K. Ackerstaff et al. (HERMES), Phys. Lett. B **475** (2000) 386.
[8] A. Airapetian et al. (HERMES), Phys. Lett. B, this volume.
[9] K. Ackerstaff et al. (HERMES), Nucl. Instr. and Meth. A **417** (1998) 230.
[10] Y.S. Tsai, Phys. Rev. **120** (1960) 269; L.W. Mo and Y.S. Tsai, Rev. Mod. Phys. **41** (1969) 205; Y.S. Tsai, SLAC-PUB-848 (1971).
[11] Review of Particle Properties, K. Hagiwara et al., Phys. Rev. D **66** (2002) 010001.
[12] A.A. Akhundov, D.Yu. Bardin and N.M. Shumeiko, Sov. J. Nucl. Phys. **26** (1977) 660; D.Yu. Bardin and N.M. Shumeiko, Sov. J. Nucl. Phys. **29** (1979) 499; and A.A. Akhundov et al., Sov. J. Nucl. Phys. **44** (1986) 988.
[13] A. Svarc and M.P. Locher, Fizika **22** (1990) 549; M.P. Locher and A. Svarc, Z. Phys. A **338** (1991) 89.
[14] J.S. McCarthy, I. Sick and R.R. Whitney, Phys. Rev. C **15** (1977) 1396.
[15] C.W. de Jager et al., Atom. Data and Nucl. Data Tables **14** (1974) 479.
[16] T. de Forest and J.D. Walecka, Adv.in Phys.15 (1966) 1.

[17] M. Gari and W. Krümpelmann, Z. Phys. A **322** (1985) 689.
[18] J. Bernabeu, Nucl. Phys. B **49** (1972) 186.
[19] E.J. Moniz et al., Phys. Rev. **184** (1969) 1154.
[20] H. Abramowicz and A. Levy, hep-ph/9712415.
[21] L.W. Whitlow et al., Phys. Lett. B **250** (1990) 193.
[22] A. Miller, in preparation.
[23] K. Kurek, Z. Phys. C **63** (1994) 561.
[24] M. Arneodo et al. (NMC), Phys. Lett. B **364** (1995) 107.
[25] S. Platchkov, Nucl. Phys. A **510** (1990) 740; P.C. Dunn et al., Phys. Rev. C **26** (1983) 71. H. de Vries et al., Atom. Data and Nucl. Data Tables **36** (1987) 501; and R.L. Huffmann et al., Phys. Lett. B **139** (1984) 249.
[26] H. Arenhövel, private communication (1998); D. Day, private communication (1998)
[27] E. Garutti, Ph.D. thesis, University of Amsterdam, in preparation (2002).
[28] P. Amaudruz et al. (NMC), Nucl. Phys. B **441** (1995) 3.
[29] M. Arneodo et al. (NMC), Nucl. Phys. B **441** (1995) 12.
[30] M. Arneodo et al. (NMC), Phys. Lett. B **481** (1996) 23.
[31] J. Gomez et al., Phys. Rev. D **49** (1994) 4348. S. Stein et al, Phys. Rev. **D 12** (1975) 1884.